Can graphene outperform indium tin oxide as transparent electrode in organic solar cells?

ARTICLE *in* 2D MATERIALS · NOVEMBER 2015

DOI: 10.1088/2053-1583/2/4/045006

6 AUTHORS, INCLUDING:

Giuseppe Iannaccone

Università di Pisa

340 PUBLICATIONS **3,368** CITATIONS

SEE PROFILE

Gianluca Fiori

Università di Pisa

120 PUBLICATIONS **1,314** CITATIONS

SEE PROFILE

Can graphene outperform indium tin oxide as transparent electrode in organic solar cells?

2015 2D Mater. 2 045006

(http://iopscience.iop.org/2053-1583/2/4/045006)

2D Materials

RECEIVED
2 July 2015

REVISED
15 September 2015

ACCEPTED FOR PUBLICATION
7 October 2015

PUBLISHED
2 November 2015

PAPER

Can graphene outperform indium tin oxide as transparent electrode in organic solar cells?

Paolo Paletti[1], **Ravinder Pawar**[1], **Giacomo Ulisse**[2], **Francesca Brunetti**[2], **Giuseppe Iannaccone**[1] and **Gianluca Fiori**[1]

[1] Dipartimento di Ingegneria dell'Informazione, Università di Pisa Via G. Caruso 16, 56122 Pisa, Italy
[2] Dipartimento di Ingegneria Elettronica, Università di Roma Tor Vergata Via del Politecnico 1, 00133 Roma, Italy

E-mail: gfiori@mercurio.iet.unipi.it

Keywords: graphene, solar cells, multi-scale simulations

Abstract

Graphene holds promises as a transparent electrode in flexible solar cells due to its high mobility and transparency. However, the experimental power conversion efficiency of cells with graphene electrode is still small (<7%). In this paper, we evaluate possible engineering options to improve the power conversion efficiency, by means of multi-scale simulation approach including ab-initio simulations of graphene contacts to improve electrode workfunction and conductance, electromagnetic simulations to improve light management, and electrical simulations of complete cells. We find that the combined effect of using a transparent electrode of graphene with a few monolayers of MoO_3 on top to optimize work function and resistivity, and of applying optimized grating to the graphene electrode, can increase power efficiency by up to 29%–47%, with respect to the ITO benchmark, depending on the material used for the hole transport layer (P3HT,PTB7, and Perovskite).

Organic semiconductor solar cells (OSCs) have recently experienced an impressive improvement in power conversion efficiency (PCE) [1]. Starting from few percentage points in 2000, they have first reduced the gap with respect to amorphous silicon solar cells, and have reached a certified 17.9% in 2014 [2].

Bulk heterojunction solar cells (BHJ-SCs) represent a promising route to low-cost, large-area cells and modules [3], since they can be manufactured at low temperature and using low cost realization processes such as printing. State-of-the-art BHJ-SCs use indium tin oxide (ITO) as a transparent electrode, which presents serious issues [4]:

- release of oxygen and indium into the organic layer, which is a reliability concern;
- poor transparency in the blue region, which limits efficiency;
- stiffness, preventing its use in flexible solar cells;
- relatively high cost due to the limited supply of indium.

To overcome these limitations, graphene electrodes have been proposed as a promising substitute to ITO [5, 6]. Indeed, graphene exhibits higher transparency than ITO [6] with an optical transparency larger than 90% [7] and exceptional electrical conductivity, which could further reduce ohmic losses [8]. However, despite the demonstration of proof-of-concept devices [9–14], the obtained power conversion efficiency is often smaller than 3%, with a recently obtained record of 7.1% [15].

Let us first briefly describe the operating principle of a BHJ-SC: In figure 1(a) the band diagram of a typical cell is shown, with the two-layers structure illustrated in figure 1(b). The two layers are organic semiconductors forming a type II heterojunction. The layer with the highest electron affinity is called the hole transport layer, or 'donor' layer, whereas the layer with the lowest electron affinity is called the electron transport layer (ETL), or 'acceptor' layer. The structure is sandwiched between two electrodes with different workfunction, in order to create a built-in electric field in the structure: the transparent electrode—in our case of ITO or graphene—has the higher workfunction and contacts the HTL, whereas the other electrode contacts the ETL.

The photogeneration mechanism in OSCs can be outlined as a four-step process as shown in figure 1(a).

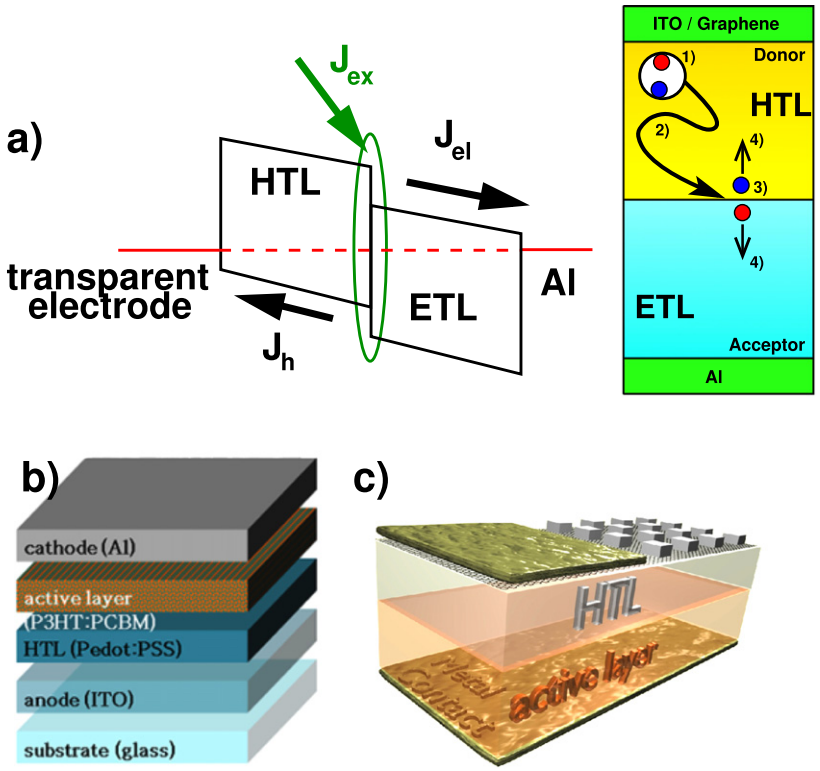

Figure 1. (a) Band diagram and sketch of the physical mechanisms playing in the OSC. (b) Device structure of a typical heterojunction OSC. (c) Simulated OSC obtained substituting ITO with graphene and considering grating of the electrode to increase optical absorption.

The absorption of a photon results in the generation of an exciton (step 1). Excitons are mobile excited states [16] that can diffuse within the active layer (step 2), with typical diffusion lengths of the order of 10 nm. At the HTL/ETL interface, due to the different electron affinity and ionization potential of the two layers, excitons rearrange in a metastable configuration known as charge-transfer state, with the electron and hole each lying in the more energetically favorable material, and eventually dissociate into free charges with specific rates (step 3). Finally, the separated holes and electrons are collected by the anode and the cathode, traveling through the HTL and ETL, respectively (step 4).

In this paper we explore the options for improving the PCE of BHJ-SCs with new materials and cell design optimization, on the basis of a multi-scale simulation approach, including ab-initio density-functional theory simulations of the graphene contacts, electromagnetic simulations of light management with a textured electrode, and device level simulation of the cell electrical characteristics.

Our main contributions are the following:

– We show that a transparent electrode of graphene with a few monolayers of MoO_3 on top can increase the PCE by up to 18%–29%, with respect to the ITO benchmark, depending on the HTL material (P3HT, PTB7, and Perovskite). Experiments have demonstrated [10] that a few monolayers of MoO_3 can provide an effective p-doping of graphene, increasing its workfunction, therefore improving charge collection and reducing the electrode resistance. We are able to achieve insights into the contact physics and to assess the PCE improvements with density functional simulations of the MoO_3-graphene interface and device level transport simulations (section 2).

– We show that a textured transparent electrode can be used to optimize light management and to increase the power density of the electromagnetic field in the active layer by up to 21%. This result is obtained with electromagnetic simulations described in section 3.

– Finally, we assess with device-level simulations the combined effect on the PCE of BHJ-SCs of using a graphene electrode with WF optimization and texture. The considered cell structure is illustrated in figure 1(c). We find that PCE can be improved of up to 47.5% in the case of P3HT active layer, 33.4% in the case of PTB7, and of 29.4% in the case of Perovskite cells, as compared to the benchmark cells with ITO electrode.

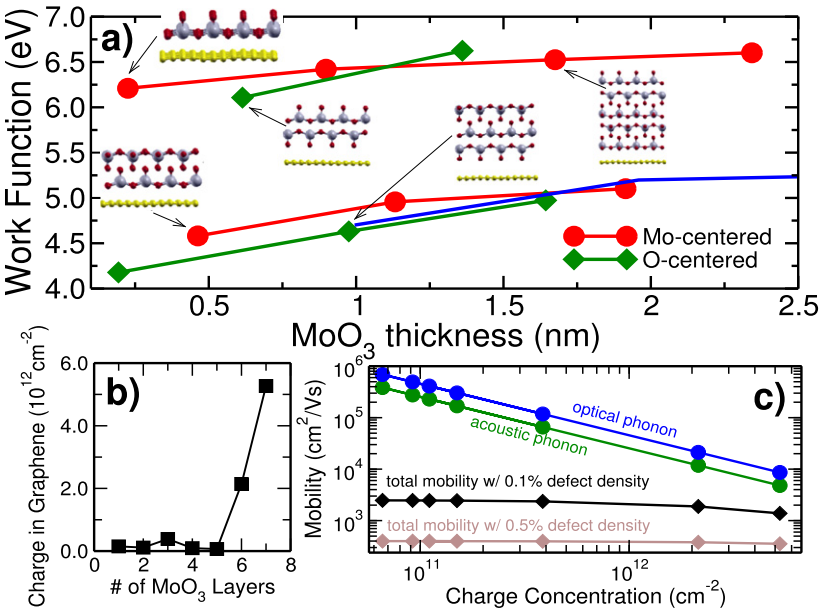

Figure 2. (a) Work-function (WF) as a function of the MoO_3 layer thickness. As shown in the insets, higher values are obtained for oxygen-terminated MoO_3 top surfaces while lower values correspond to Mo-terminated surfaces. The solid line represents experiments from [10]. (b) Charge density in the graphene sheet as a function of the number of MoO_3 layers. (c) Carrier mobility *vs* charge density for different scattering mechanisms.

1. Engineering of the organic solar cell with graphene transparent electrode

In this section we focus on understanding how a few layers of MoO_3 on top of the graphene layer can enable workfunction engineering, and how this option can be used to optimize device performance. We believe that the deposition of MoO_3 is one of the most promising technologies in order to tune graphene work-function. As indeed we will show, only few nanometers of MoO_3 are necessary in order to dope graphene, preserving the morphology of the texturing needed to improve light adsorbance. In addition, MoO_3 can be deposited through thermal evaporation process, which allows the thickness of the deposited material to be precisely controlled.

In order to do so, we need a multi-physics approach using density-functional theory simulations of the graphene/MoO_3 contact and device-level simulations, self-consistently solving electrostatics and charge transport.

Performance is evaluated in terms of the main figures of merit, i.e., the open-circuit voltage V_{oc}, the short-circuit current J_{sc}, the fill factor *FF* and the power conversion efficiency PCE, using as a benchmark the cell with the ITO transparent electrode.

As demonstrated in [10], depositing MoO_3 on graphene leads to a WF tuning: the larger the MoO_3 thickness, the larger the WF.

To understand this aspect, we investigated the graphene/MoO_3 interface with DFT simulations, as a function of MoO_3 thickness and considering two different MoO_3 structures: as shown in the inset of figure 2(a), the O-centered structure has oxygen atoms closer to the graphene surface, whereas the Mo-centered structure has molybdenum atoms closer to graphene.

In figure 2(a), we show the WF computed with DFT as a function of MoO_3 thicknesses and for the different geometries. As can be seen, two families of WFs appear in the figure: one with values ranging from 6.2 to 6.5 eV, corresponding to an oxygen-terminated MoO_3 top surface (red atoms), and one with values ranging from 4.2 to 5.2 eV, corresponding to a Mo-terminated top surface (gray atoms). Indeed, the electronegativity of oxygen is 3.44 eV, whereas that of Mo is 2.16 eV. As a consequence, larger energy is required to extract one electron from the O-terminated MoO_3.

In the same plot, we show the experimental results [10], that are in good agreement with simulations of Mo-terminated structures. We explain this agreement by considering that—in experimental samples—deposited MoO_3 likely consists of many domains with different structures and orientation. From simulations, we find that Mo-terminated structures have the lowest WF, therefore determine the experimental WF, as obtained by means of Ultraviolet Photoelectron Spectroscopy [10].

A higher WF translates in a higher built-in electric field in the cell and therefore a higher charge collection efficiency, which tends to improve the PCE. In addition, a higher WF implies a higher hole density (as shown in figure 2(b)) and suppressed mobility in graphene [17], which have a counteracting effect on the series resistance of the contact, and therefore on PCE.

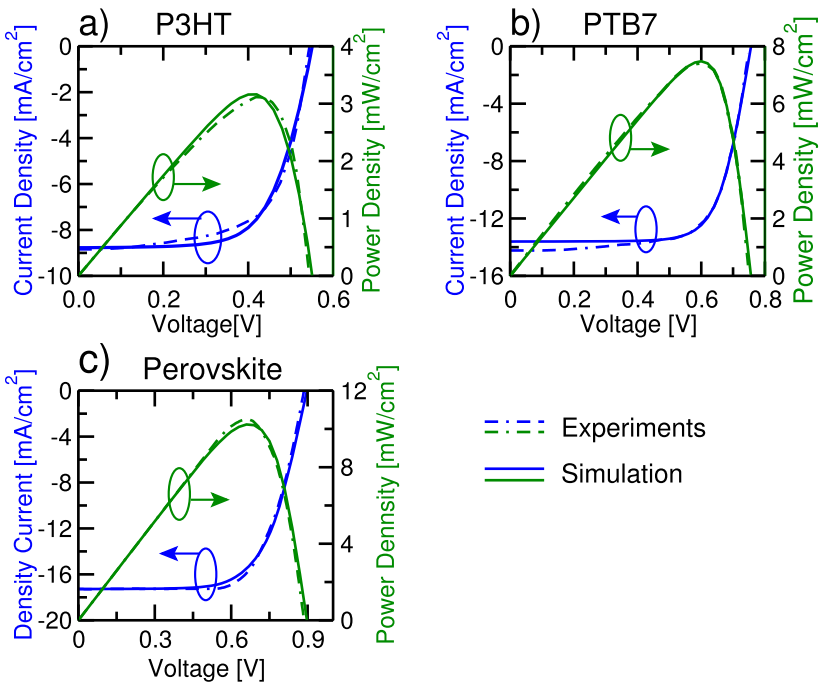

Figure 3. Calibration of the drift-diffusion model (solid lines) with experimental data (dashed lines) on OSCs with (a) P3HT (our experiments), (b) PTB7 [23] and (c) Perovskite [24] as HTL and ITO top electrode.

We have evaluated mobility considering the main scattering mechanisms, i.e., electron-phonon scattering (both acoustic and optical), and the presence of defects (vacancies) [18] (figure 2(c)).

Mobilities limited by acoustic and optical phonons (μ_{ac} and μ_{op}, respectively) have been evaluated as follows [17, 19]

$$\mu_{ac} = \frac{q\rho_m \hbar v_F^2 v_{ph}^2}{4\pi D_{ac}^2} \frac{1}{\rho K_B T}, \quad (1)$$

$$\mu_{op} = \frac{q\rho_m v_F^2 \omega_{op}}{2\pi D_{op}^2} \frac{1}{\rho N_{op}}, \quad (2)$$

where q is the elementary charge, ρ_m is the mass density, T is the temperature, v_F is the Fermi velocity, v_{ph} is the sound velocity, N_{op} the optical phonon occupation factor, D_{ac} (D_{op}) is the acoustic (optical) deformation potential. The charge density in graphene (ρ) has been computed through DFT calculations (figure 2(b)). As can be seen from 1 and 2, the product $(\mu_{ac} + \mu_{op})\rho$ is a constant, and provides a contact resistance of 200 Ω sq^{-1}, comparable to ITO, independent of the WF.

However, the situation is different if we consider a small percentage of defects (vacancies or grain-boundaries). For state-of-the-art graphene technology, mobility is limited by defects, as shown in figure 2(c) for a relatively low defect density. In this case, total mobility has a very small dependence on charge concentration, and an increase of the WF, and therefore of hole density, can greatly suppress the contact resistance.

To quantitatively assess the achievable gain in PCE, and to provide design guidelines for the fabrication of OSCs, we have investigated the sensitivity of the main OSC figures of merit on OSC parameters (e.g., graphene electrode work-function and active layer material). To this purpose, we have performed simulations at the device level, similarly to what was done in [20–22], while exploiting the information obtained at the atomic level through DFT calculations.

First, we have calibrated our device model and materials parameters, by performing simulations of OSCs with P3HT, PTB7 and Perovskite HTL and ITO as transparent electrode, and comparing the obtained $I-V$ characteristics with experimental results (figure 3).

Simulation results nicely agree with experiments using only few basic model parameters: the width of the region in correspondence of the interface where excitons are generated W_{int}, the carrier mobilities (μ_n and μ_p), and the difference between the conduction band of the acceptor layer $LUMO_A$ and the valence band of the donor layer $HOMO_D$. The considered parameters are shown in the supplementary material.

We have then performed the same simulations with the graphene electrode in the place of ITO, exploring the parameter space. In figure 4, we plot the fill factor and the efficiency, as a function of WF and contact resistance, for different materials for the HTL (P3HT, PTB7, and Perovskite, respectively). For the work-function, we have considered the energy interval extracted from DFT calculations, when evaluating WF for the different MoO_3 thicknesses.

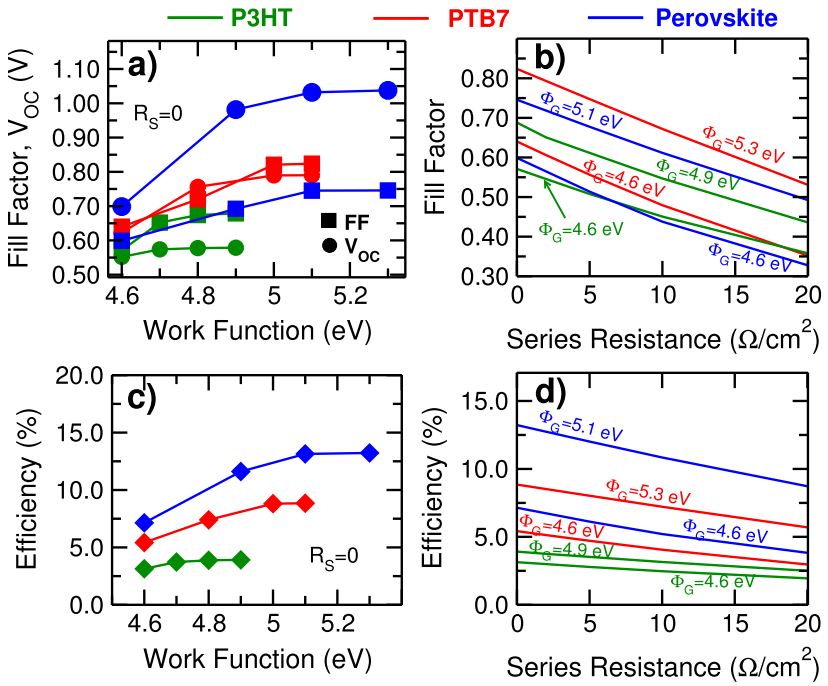

Figure 4. Figures of merit of OSCs for different materials for the active layers, i.e., P3HT (green lines), PTB7 (red lines) and Perovskite (blue lines). (a) Fill Factor and V_{oc} and (c) efficiency as a function of electrode work function, for a series resistance equal to zero; (b) Fill Factor and (d) efficiency different electrode work functions as a function of the series resistance.

It is apparent that both series resistance and the work function play an important role in the OSC performance improvement. For all the considered materials, the FF, V_{oc}, and the efficiency increase with increasing work function. However, all the above considered figures of merit rapidly saturate, as shown in figures 4(a) and (c), leading to a reduced sensitivity to WF tuning.

From figures 4(b) and (d), we note that OSCs are extremely sensitive to the series resistance per unit cell area, which depends upon the electrode sheet resistance and the layout geometry. From a fabrication point of view, this means that particular attention has to be paid both to increase the WF and to limit the number of defects and grain boundaries, so to reduce the overall resistance of the graphene electrode.

2. Light management with textured electrode

In this section we focus on further improvements obtained with light management in BHJ-SCs, using a textured transparent electrode. We show in figure 5(a) the considered electrode grating, highlighting the grating pitch, and in figures 5(b)-(c) the cross-section of the simulated OSCs. The layer stack and the materials are those considered in the electrical simulations of the previous section. In addition, we have simulated an active layer patterning, to form square pillars above which the graphene/MoO_3 layer adheres.

A glass is also considered on top of the graphene electrode. The other electrode is made of aluminum.

The simulations of the OSC have been performed by means of the electromagnetic tool of the Comsol Multiphysics package [25], which allows the calculation of the electric field distribution inside the active layer, and the generation rate [26, 27] in 3D structures.

We focus on the optimization of the so-called *enhancement factor* (EF), defined as the ratio of the generation rate of a textured graphene OSC to the generation rate of an OSC with a flat architecture with the same active layer thickness. As input signal, we have considered the Sun irradiation spectrum intensity of standard air mass 1.5(AM 1.5) [28]. In order to perform accurate simulations, both the real and the complex part of the refractive index of the considered OSC materials is needed, and typically obtained from spectroscopy ellipsometry measurements [29–33].

For graphene, we have considered the refractive index measurements available in the literature [34]. The OSCs have been simulated considering a single period of grating and applying periodic boundary conditions along the in-plane directions.

In figures 5(d)-(e) the colormap of the generation rate distribution for the optimized grating geometry is shown. The introduction of the grating leads to a strong concentration of absorbed photons in correspondence of the region between two pillars, and therefore to an increase of the generation rate. As can be seen in figure 6, an enhancement factor of 21% can be obtained in a P3HT:PCBM OSC with grated electrode.

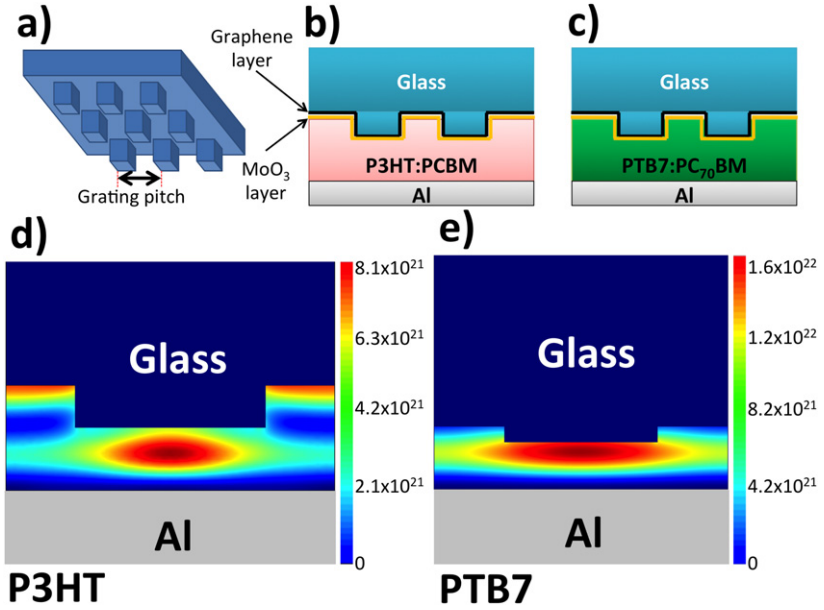

Figure 5. (a) Grated electrode with graphene and MoO_3 layers sandwiched between the glass substrate and the (b) P3HT:PCBM and (c) PTB7:PC_{70}BM active layers; (d), (e): generation rate density in the cases of (b) and (c), respectively.

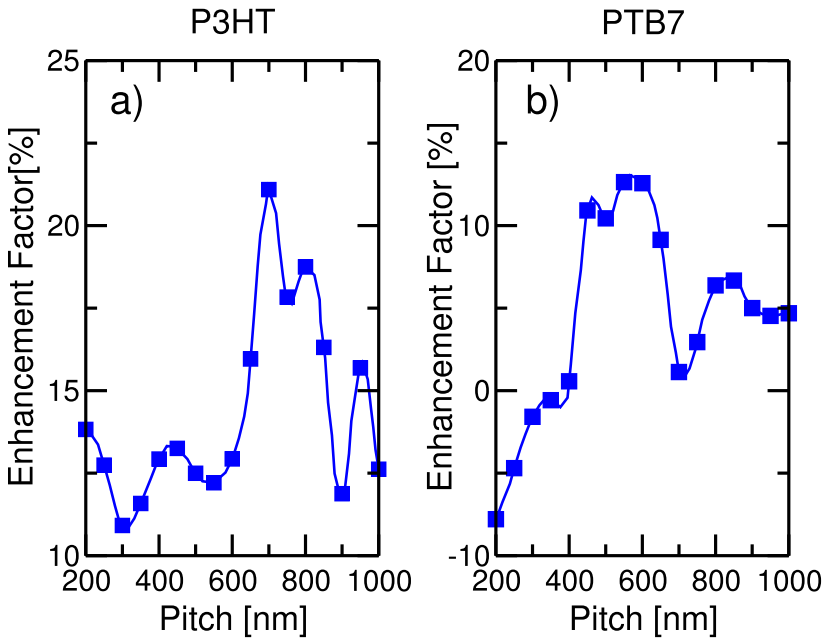

Figure 6. Enhancement Factor as a function of the grating pitch for a) P3HT- and b) PTB7-based OSC. EF is the ratio of the number of generated excitons in the presence of grating to the same number in the absence of grating.

In figure 7, we show PCE and J_{sc} as a function of WF for OSC with P3HT:PCBM and PTB7:PC_{7O}BM as active layer, with and without electrode grading. As can be seen, J_{sc} is almost independent on WF tuning. Grating can lead to an improvement of both J_{sc} and PCE of 20%.

Finally, we compare in figure 8 the efficiency of cells with different HTL materials and the efficiency improvement provided by each cell engineering option, using as a benchmark cells with the ITO transparent electrode. All results are based on our multiscale simulation approach: we have performed electrical simulations of the cells with NanoTCAD ViDES [35] including results from ab-initio simulations of contacts and from electromagnetic simulations. As can be seen, low contact resistance, work function tuning, and electrode grating can jointly provide a boost in power conversion efficiency of up to 30% with respect to the benchmark cells.

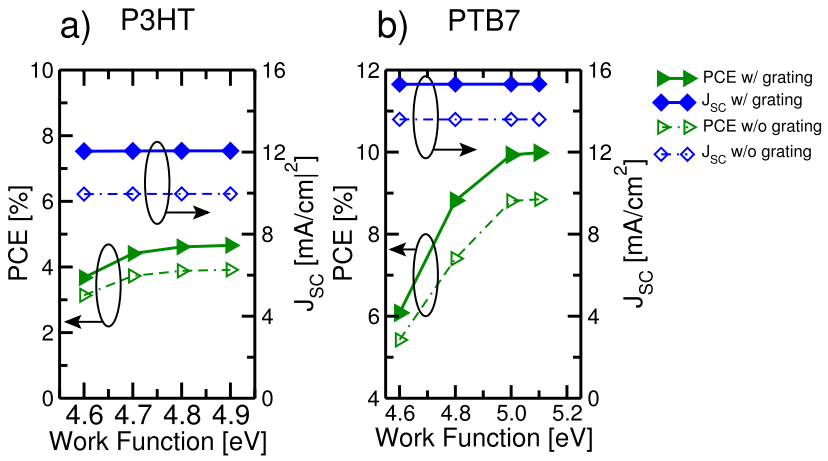

Figure 7. Effect of grating on the short-circuit current and hence the efficiency for (a) P3HT- and (b) PTB7-based OSC.

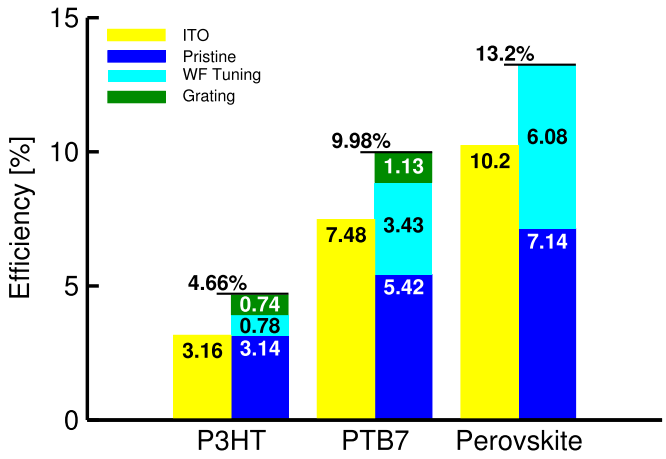

Figure 8. PCE of the investigated OSC with graphene transparent electrode showing improved performance of 47.5%, 33.4% and 29.4% with respect to their ITO counterparts for P3HT (our experiments), PTB7 [23] and Perovskite [24], respectively.

3. Conclusion

We have performed, for the first time, a detailed investigation of the performance of graphene-based flexible organic solar cell, by means of a multi-scale approach including quantum chemistry simulations to optimize graphene contacts, electromagnetic simulations to optimize light management, and electrical simulations at the cell level. Graphene OSCs can exhibit better performance as compared to ITO counterpart, if series resistance of the contact is minimized (e.g. if high-quality graphene is used), and if the workfunction is optimized in order to reduce series resistance and induce a higher built-in electric field in the cell. Further improvement can be obtain with graphene electrode grating. The same techniques can also be used with the new and promising Perovskite materials for achieving record efficiency.

Acknowledgments

Authors gratefully acknowledge the support from the EC. 7FP through the Project GONEXTs (Contract 309201), Quantavis s.r.l. and support from the Graphene Flagship (Contract 604391). Computational resources at nanohub.org are gratefully acknowledged.

References

[1] You J, Dou L, Hong Z, Li G and Yang Y 2013 Recent trends in polymer tandem solar cells research *Progr. Polymer Sci.* **38** 1909–28

[2] Ryu S, Noh J H, Jeon N J, Kim Y C, Yang W S, Seo J W and Seok S I 2014 Voltage output of efficient Perovskite solar cells with high open-circuit voltage and fill factor *Energy Env. Sci.* doi:10.1039/C4EE00762J

[3] Dennler G, Scharber M C and Brabec C J 2009 Polymer-Fullerene bulk-heterojunction solar cells *Adv. Mater.* **21** 1323–38

[4] Schlatmann A, Floet D W, Hilberer A, Garten F, Smulders P, Klapwijk T and Hadziioannou G 1996 Indium contamination from the indiumtinoxide electrode in polymer light-emitting diodes. *Appl. Physics Lett.* **69** 1764–6
[5] Shi Y, Kim K K, Reina A, Hofmann M, Li L-J and Kong J 2010 Work function engineering of graphene electrode via chemical *ACS Nano* **4** 2689–94 PMID: 20433163
[6] Koh W S, Gan C H, Phua W K, Akimov Y A and Bai P 2014 The potential of graphene as an ITO replacement in organic solar cells: An optical perspective *IEEE J.Quantum Electr.* **20** 36–42
[7] Nair R, Blake P, Grigorenko A, Novoselov K, Booth T, Stauber T, Peres N and Geim A 2008 Fine structure constant defines visual transparency of graphene *Science* **320** 1308–1308
[8] Geim A K and Novoselov K S 2007 The rise of graphene. *Nat. mater.* **6** 183–91
[9] Wang Y, Tong S W, Xu X F, Ozyilmaz B and Loh K P 2011 Interface engineering of layer-by-layer stacked graphene anodes for high-performance organic solar cells *Adv.Mater.* **23** 1514–8
[10] Tong S W, Wang Y, Zheng Y, Ng M-F and Loh K P 2011 Graphene intermediate layer in tandem organic photovoltaic cells *Adv. Funct. Mater.* **21** 4430–5
[11] Liu Z, Li J, Sun Z-H, Tai G, Lau S-P and Yan F 2012 The application of highly doped single-layer graphene as the top electrodes of semitransparent organic solar cells *ACS Nano* **6** 810–8 PMID: 22148872
[12] Park H, Brown P R, Bulovic V and Kong J 2012 Graphene as transparent conducting electrodes in organic photovoltaics: studies in graphene morphology, hole transporting layers, and counter electrodes *Nano Letters* **12** 133–40 PMID: 22107487
[13] Khrapach I, Withers F, Bointon T H, Polyushkin D K, Barnes W L, Russo S and Craciun M F 2012 Novel highly conductive and transparent graphene-based conductors *Adv. Mater.* **24** 2844–9
[14] Park H, Howden R M, Barr M C, Bulovic V, Gleason K, Kong J and Nano A C S 2012 Organic solar cells with graphene electrodes and vapor printed poly(3, 4-ethylenedioxythiophene) as the hole transporting layers *ACS Nano* **6** 6370–7 PMID: 22724887
[15] Park H, Chang S, Zhou X, Kong J, Palacios T and Gradečak S 2014 Flexible graphene electrode-based organic photovoltaics with record-high efficiency *Nano Letters* **14** 5148–54 PMID: 25141259
[16] Gregg B A and Hanna M C 2003 Comparing organic to inorganic photovoltaic cells: Theory, experiment, and simulation *J. Appl. Phys.* **93** 3605–14
[17] Shishir R S and Ferry D K 2009 Velocity saturation in intrinsic grapheneJ. *Phys.: Condensed Matt.* **21** 344201
[18] Betti A, Fiori G and Iannacone G 2011 Strong mobility degradation in ideal graphene nanoribbons due to phonon scattering *Appl. Phys. Lett.* **98** 212111
[19] Perebeinos V and Avouris P 2010 Inelastic scattering and current saturation in graphene *Phys. Rev.* B **81** 195442
[20] Ray B and Alam M 2013 Achieving fill factor above 80 charged interface *IEEE J. Photovoltaics* **3** 310–7
[21] Ray B, Nair P R and Alam M A 2011 Annealing dependent performance of organic bulkheterojunction solar cells: A theoretical perspective *Sol. Energy Mater. Sol. Cells* **95** 3287 – 3294
[22] Ray B and Alam M A 2011 A compact physical model for morphology induced intrinsic degradation of organic bulk heterojunction solar cell. *Appl. Phys. Lett.* 99
[23] Liang Y, Xu Z, Xia J, Tsai S-T, Wu Y, Li G, Ray C and Yu L 2010 For the bright futurebulk heterojunction polymer solar cells with power conversion efficiency of 7.4%. *Adv. Mater.* **22** 135–8
[24] You J *et al* 2014 Low-temperature solution-processed Perovskite solar cells with high efficiency and flexibility *ACS Nano* **8** 1674–80 PMID: 24386933
[25] Info available at http://comsol.com
[26] Park W 2013 Combined optical and electrical modeling of plasmon-enhanced organic photovoltaic devices *Renewable Energy and the Environment* pp PW3B–5
[27] Fallahpour A, Ulisse G, Auf der Maur M, di Carlo A and Brunetti F 2014 3-D simulation and optimization of organic solar cell With periodic back contact grating electrode *IEEE J. Photovoltaics* **5** 591–6
[28] www.astm.org/Standards/G173.htm
[29] Synowicki R 1998 Spectroscopic ellipsometry characterization of indium tin oxide film microstructure and optical constants *Thin Solid Films* **313** 394–7
[30] Hoppe H, Sariciftci N and Meissner D 2002 Optical constants of conjugated polymer/fullerene based bulk-heterojunction organic solar cells *Molecular Crystals and Liquid Crystals* **385** 113–9
[31] You J, Li X, Xie F-x, Sha W E, Kwong J H, Li G, Choy W C and Yang Y 2012 Surface plasmon and scattering-enhanced low-bandgap polymer solar cell by a metal grating back electrode *Advanced Energy Materials* **2** 1203–7
[32] Monestier F, Simon J-J, Torchio P, Escoubas L, Flory F, Bailly S, de Bettignies R, Guillerez S and Defranoux C 2007 Modeling the short-circuit current density of polymer solar cells based on P3HT: PCBM blend *Solar Energy Materials and Solar Cells* **91** 405–10
[33] Szekeres A, Ivanova T and Gesheva K 2002 Spectroscopic ellipsometry study of CVD molybdenum oxide films: effect of temperature *J. Solid State Electrochem.* **7** 17–20
[34] Weber J, Calado V and van de Sanden M 2010 Optical constants of graphene measured by spectroscopic ellipsometry *Appl. Phys. Lett.* **97** 091904
[35] Fiori G and Iannaccone G 2013 Multiscale modeling for graphene-based nanoscale transistors *Proc. IEEE* **101** 1653–69